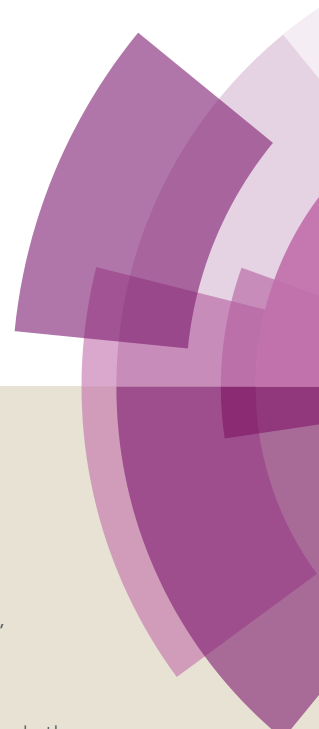


Dalton Transactions

Accepted Manuscript



This article can be cited before page numbers have been issued, to do this please use: Y. Dong, R. Fan, W. Chen, H. Zhang, Y. Song, X. Du, P. Wang, L. Wei and Y. Yang, *Dalton Trans.*, 2016, DOI: 10.1039/C6DT04159K.



This is an Accepted Manuscript, which has been through the Royal Society of Chemistry peer review process and has been accepted for publication.

Accepted Manuscripts are published online shortly after acceptance, before technical editing, formatting and proof reading. Using this free service, authors can make their results available to the community, in citable form, before we publish the edited article. We will replace this Accepted Manuscript with the edited and formatted Advance Article as soon as it is available.

You can find more information about Accepted Manuscripts in the [author guidelines](#).

Please note that technical editing may introduce minor changes to the text and/or graphics, which may alter content. The journal's standard [Terms & Conditions](#) and the ethical guidelines, outlined in our [author and reviewer resource centre](#), still apply. In no event shall the Royal Society of Chemistry be held responsible for any errors or omissions in this Accepted Manuscript or any consequences arising from the use of any information it contains.



Journal Name

ARTICLE

Different Conjugated System Zn(II) Schiff Base Complexes: Supramolecular Structure, Luminescent Properties and Application in PMMA-Doped Hybrid Material

Received 00th January 20xx,
Accepted 00th January 20xx

DOI: 10.1039/x0xx00000x

www.rsc.org/

Yu-Wei Dong, Rui-Qing Fan,* Wei Chen, Hui-Jie Zhang, Yang Song, Xi Du, Ping Wang, Li-Guo Wei, and Yu-Lin Yang,*

A series of Zn(II) complexes with different conjugated system, $[\text{ZnL}^1\text{Cl}_2]_2$ (**Zn1**), $[\text{ZnL}^2\text{Cl}_2]$ (**Zn2**), $[\text{Zn}(\text{L}^3)_2](\text{ClO}_4)_2$ (**Zn3**), $[\text{Zn}_2\text{L}^4\text{Cl}_4]$ (**Zn4**), $[\text{ZnL}^5\text{Cl}_2]$ (**Zn5**) have been synthesized and subsequently characterized by single crystal X-ray diffraction, ^1H and ^{13}C NMR, FT-IR, elemental analyses, melting point, and PXRD. The X-ray diffraction analyses revealed that the supramolecular frameworks of complexes **Zn1–Zn5** are constructed by C–H \cdots O/Cl hydrogen bonds and $\pi\cdots\pi$ interactions. Complexes **Zn1–Zn3** feature 3D 6-connected $\{4^{12}\cdot 6^3\}$ topology structures, while complex **Zn4** exhibits 3D 7-connected supramolecular framework with $\{4^{17}\cdot 6^4\}$ topology structure. Complex **Zn5** shows one-dimensional “wave-like” chains. Based on these varied structure, the emission maximum wavelengths of complexes **Zn1–Zn5** can be tuned in a large range of 461–592 nm due to the red shift direction of λ_{em} causing by different conjugated system and their electron donating ability. Specially, complex **Zn3** shows strong luminescence in the solid state and acetonitrile solvent. Therefore, a series of **Zn3**-poly(methylmethacrylate) (**Zn3**-PMMA) hybrid materials are obtained through controlling the concentration of complex **Zn3** in poly(methylmethacrylate) (PMMA). At a optical concentration of 4%, the doped polymer film of **Zn3**-PMMA displays a strong and green luminescence emissions, which is 19-fold in the luminescence intensities and 98 °C higher in the thermal stability temperature compared with that of **Zn3**.

Introduction

Even since the discovery of supramolecular chemistry, the chemistry of noncovalent interactions has experienced tremendous growth.^{1–5} It has been applied in many research fields with important implications in chemistry, physics, material science, engineering and medicine.^{6–15} Since the incorporation of well-ordered structural components into a crystal lattice may lead to new advanced materials with designed physico-chemical properties, such work will provide a foundation for the understanding of how molecules can be organized and how functions are revealed. Meanwhile, many efforts have been devoted to the use of supramolecular contacts, such as hydrogen bonds, $\pi\cdots\pi$, C–H $\cdots\pi$, aromatic ring \cdots halogen, and/or other van der Waals interactions,^{16–21} which play important roles in the

construction of ordered supramolecular architectures. Schiff base ligands are frequently used in coordination chemistry due to their significant ability to form stable complexes with metal ions.^{22–25} Zinc Schiff base complexes with luminescent properties can be used in applications involving fabrication of novel materials and as probes in biological systems.^{26–31} Controllable tuning of fluorescent properties of zinc complexes based on ligand design is always a challenge for chemists. From the viewpoint of molecular and crystal engineering, the critical criterion for ligand design is how to embed noncovalent interaction groups to control the molecular structure and the supramolecular framework.

Schiff base complexes doped with PMMA as a high performance luminescent materials are rare.³² What's more, the idea that greenish luminescence Schiff base complexes doped with PMMA using in plastic greenhouses could increase leaf photosynthesis has never been reported. Polymer-doped systems have obvious technical advantages, such as flexibility and prominent processing ability, which are important for optical fibers and fiber amplifiers.^{33,34} In recent years, polymer-doped systems are mainly on the rare earth complexes doped with PMMA, however, the lower synthetic yields, higher costs, larger doping amount and single luminous color restrict

MIIT Key Laboratory of Critical Materials Technology for New Energy Conversion and Storage, School of Chemistry and Chemical Engineering, Harbin Institute of Technology, Harbin 150001 (P. R. China) E-mail: fanruiqing@hit.edu.cn, ylyang@hit.edu.cn; Fax: +86-451-86418270

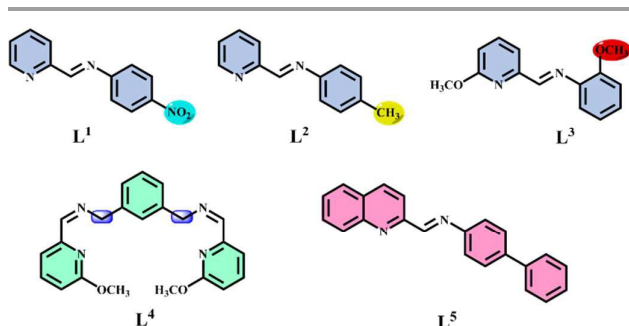
Electronic Supplementary Information (ESI) available: X-ray crystallographic files, CCDC 1508968–1508972 for **Zn1–Zn5**, IR, ^1H NMR, ^{13}C NMR, elemental analyses, melting point, PXRD, UV-vis, TGA. For ESI and crystallographic data in CIF or other electronic see DOI: 10.1039/x0xx00000x

ARTICLE

Journal Name

economic benefit and waste resources.³⁵ In this work, lower costs Zn(II) metal salts are selected to successfully synthesize higher synthetic yields, strong luminescence Schiff base complexes. Remarkably, the availability of Zn(II) complex doped with PMMA as a high performance luminescent materials.

In line with the above discussion and the fact that the type of substituents and conjugated system are the main factors to affect the supramolecular frameworks and luminescent properties, five Schiff base ligands, **L**¹–**L**⁵, Scheme 1, carrying different substitutions and conjugated system have been employed for the synthesis of Zn(II) complexes. Five Zn(II) complexes, namely **Zn1**–**Zn5**, were prepared by the reactions of corresponding ligand and ZnCl₂/Zn(ClO₄)₂, which display luminescence ranging from blue to yellow. The optical properties of all the complexes were investigated by UV-vis absorption and luminescence spectroscopy in solution and in the solid state. After doping complex **Zn3** with PMMA at the concentration of 4% (**Zn3**-PMMA), the luminescence intensities of the polymer film material **Zn3**-PMMA increase 19-fold and its thermal stability temperature raised 98 °C compared with those of **Zn3**.



Scheme 1. Structures of Schiff base ligands **L**¹–**L**⁵.

Experimental Section

Materials and instrumentation

All reagents and solvents were purchased from commercial sources and were used without further purification. Elemental analyses were carried out on a Perkin–Elmer 2400 automatic analyzer. FT–IR spectra data (4000–400 cm^{−1}) were collected by a Nicolet impact 410 FT–IR spectrometer. ¹H NMR spectra were obtained using a Bruker Avance–400 MHz spectrometer with Si(CH₃)₄ as internal standard. ¹³C NMR (150 MHz) spectra were recorded on a Bruker Avance-600 spectrometer. Melting points were determined using a capillary melting point apparatus and are uncorrected. Powder X-ray diffraction (PXRD) patterns were recorded in the 2θ range of 5–50° using Cu–Kα radiation by Shimadzu XRD-6000 X-ray Diffractometer. The thermal analyses were performed on a ZRY-2P thermogravimetric analysis under a flow of air from room temperature to 700 °C. A Perkin–Elmer Lambda 35 spectrometer was used to measure the UV–vis absorption spectra of ligands and complexes. The emission luminescence and lifetime properties were recorded with Edinburgh FLS 920 fluorescence spectrometer. Lifetime studies were performed using photon-counting system with a microsecond pulse lamp as the excitation source. The emission decays were analyzed by the sum of exponential functions. The

decay curve is well fitted into a double exponential function:³⁶ $I(t) = A_1 \exp(-t/\tau_1) + A_2 \exp(-t/\tau_2)$, where I is the luminescence intensity, and τ_1 and τ_2 are the lifetimes for the exponential components. The average lifetimes were calculated with Equation (1).

$$\frac{\tau_1^2 A_1 \% + \tau_2^2 A_2 \%}{\tau_1 A_1 \% + \tau_2 A_2 \%} \quad (1)$$

Quinine sulfate in 0.1 M H₂SO₄ (quantum yield 0.546 at 350 nm) was chosen as a standard.^{37–39} The absolute values were calculated from the fixed and known fluorescence quantum yield of the standard reference sample through Equation (2).

$$Q = Q_R \frac{I}{I_R} \frac{OD_R}{OD} \frac{n^2}{n_R^2} \quad (2)$$

In Equation (2), Q is the quantum yield, I is the measured integrated emission intensity, n is the refractive index, and OD is the optical density. The subscript R refers to the reference fluorophore of known quantum yield. In order to minimize re-absorption effects absorbencies in the 10 mm fluorescence cuvette were kept under 0.05 at the excitation wavelength (350 nm).

X-ray crystallography

Suitable crystals of complexes **Zn1**–**Zn5** were selected and mounted on a Rigaku R–AXIS RAPID IP diffractometer. Diffraction data were collected using graphite-monochromatized Mo–Kα radiation ($\lambda = 0.71073 \text{ \AA}$). The structures were solved with direct methods⁴⁰ and refined with full–matrix least–squares on F^2 . All the hydrogen atoms were constrained in geometric positions to their parent atoms and non-hydrogen atoms were refined anisotropically. The detailed crystal structure refinement data are given in Table 1, selected bond lengths and angles are listed in Tables S1–S2†. The CCDC numbers are 1508968–1508972 for **Zn1**–**Zn5**, respectively.

Synthesis of the ligands and complexes

(E)-4-nitro-*N*-((pyridin-2-yl)methylene)aniline (**L**¹). 2-pyridinecarboxaldehyde (1.40 mL, 14.72 mmol) and 4-nitroaniline (2.00 g, 14.46 mmol) were dissolved in the mixed solutions of anhydrous methanol (20 mL) and tetrahydrofuran (25 mL), the resulting mixture was heated at reflux temperature for 11 h. The solvent was removed under reduced pressure to give yellow powders. M.p. = 130.2–131.5 °C. Yield: 2.22 g (67%). Anal. Calcd (%) for C₁₂H₉N₃O₂ ($M = 227.22 \text{ g mol}^{-1}$): C, 63.43; H, 3.99; N, 18.49. Found: C, 63.38; H, 3.41; N, 18.45. FT-IR bands (KBr, cm^{−1}): $\nu_{C=N}$ 1630 (m). ¹H NMR (400 MHz, CDCl₃): δ 8.79 (d, $J = 4.8 \text{ Hz}$, 1H, Py-*H*₆), 8.61 (s, 1H, CH=N), 8.31 (d, $J = 8.4 \text{ Hz}$, 1H, Py-*H*₃), 8.08 (d, 2H, $J = 8.8 \text{ Hz}$, Ph-*H*_{3,5}), 7.93 (t, 1H, $J = 7.6 \text{ Hz}$, Py-*H*₄), 7.57 (t, 1H, $J = 7.2 \text{ Hz}$, Py-*H*₅), 6.66 (d, 2H, $J = 9.2 \text{ Hz}$, Ph-*H*_{2,6}) ppm. ¹³C NMR (150 MHz, CDCl₃): δ 163.31, 152.52, 150.26, 139.12, 137.13, 127.94, 126.39, 125.12, 121.42, 113.38 ppm.

(E)-4-methyl-*N*-((pyridin-2-yl)methylene)aniline (**L**²). 2-pyridinecarboxaldehyde (1.52 mL, 15.98 mmol) and 4-methylaniline (1.77 mL, 15.88 mmol) were dissolved in 20 mL of anhydrous methanol and the resulting mixture was heated at reflux temperature for 3 h. The solvent was removed under reduced pressure and the residue was recrystallized from the mixed solvent of *n*-hexane and

dichloromethane to give yellow crystals. M.p. = 67.5–68.7 °C. Yield: 2.79 g (90%). Anal. Calcd (%) for $C_{13}H_{12}N_2$ ($M = 196.25 \text{ g mol}^{-1}$): C, 79.56; H, 6.16; N, 14.27. Found: C, 79.55; H, 6.17; N, 14.28. FT-IR bands (KBr, cm^{-1}): $\nu_{\text{C=N}}$ 1628 (m). $^1\text{H NMR}$ (400 MHz, CDCl_3): δ 8.74 (d, 1H, $J = 4.4 \text{ Hz}$, Py- H_6), 8.65 (s, 1H, CH=N), 8.24 (d, 1H, $J = 8.0 \text{ Hz}$, Py- H_3), 7.84 (t, $J = 7.6 \text{ Hz}$, 1H, Py- H_4), 7.40 (t, $J = 5.6 \text{ Hz}$, 1H, Py- H_5), 7.00 (d, 2H, $J = 8.4 \text{ Hz}$, Ph- $H_{2,6}$), 7.00 (d, 2H, $J = 7.6 \text{ Hz}$, Ph- $H_{3,5}$), 2.41 (s, 3H, Ph- CH_3) ppm. $^{13}\text{C NMR}$ (150 MHz, CDCl_3): δ 159.63, 154.68, 149.63, 148.31, 136.81, 136.71, 129.87, 125.01, 121.82, 121.12, 21.08 ppm.

(*E*)-2-methoxy-*N*-((6-methoxypyridin-2-yl)methylene)aniline (\mathbf{L}^3). A mixture of 2-methoxyaniline (1.90 g, 16.94 mmol) and 6-methoxy-2-pyridinecarboxaldehyde (2.0 mL, 16.63 mmol) was refluxed in anhydrous methanol (30 mL) in the presence of a catalytic amount of formic acid for 12 h. After the reaction was over, the resulting solution was concentrated under reduced pressure (oil pump) to obtain brown yellow oil. Then the brown yellow residue was recrystallized from *n*-hexane solvent to give yellow solids. M.p. = 55.0–56.3 °C. Yield: 4.03 g (89 %). Anal. Calcd for $C_{14}H_{14}N_2O_2$ ($M = 242.27 \text{ g mol}^{-1}$): C, 69.41; H, 5.82; N, 11.56 %. Found: C, 69.17; H, 5.99; N, 11.38 %. FT-IR bands (KBr, cm^{-1}): $\nu_{\text{C=N}}$ 1632 (m). $^1\text{H NMR}$ (400 MHz, CDCl_3): δ 8.50 (s, 1H, CH=N), 7.85 (d, 1H, $J = 7.2 \text{ Hz}$, Py- H_5), 7.73 (t, 1H, $J = 8.0 \text{ Hz}$, Py- H_4), 7.56 (d, 1H, $J = 7.2 \text{ Hz}$, Py- H_3), 7.22 (t, 1H, $J = 7.2 \text{ Hz}$, Ph- H_4), 7.09 (d, 1H, $J = 7.2 \text{ Hz}$, Ph- H_6), 6.83 (d, 1H, $J = 8.0 \text{ Hz}$, Ph- H_3), 6.73 (t, 1H, $J = 5.6 \text{ Hz}$, Ph- H_5), 4.03 (s, 3H, Py- OCH_3), 3.99 (s, 3H, Ph- OCH_3) ppm. $^{13}\text{C NMR}$ (150 MHz, CDCl_3): δ 163.68, 152.02, 150.60, 138.99, 128.07, 126.88, 123.93, 121.86, 118.17, 116.38, 114.10, 112.78, 54.30, 53.50 ppm.

N,N'-bis(6-methoxy-2-pyridinylmethylene)phenylene-1,3-dimethanamine (\mathbf{L}^4). 6-methoxy-2-pyridinecarboxaldehyde (1.80 mL, 15.00 mmol) and 1,3-benzenedimethanamine (1.00 mL, 7.50 mmol) were dissolved in 25 mL of anhydrous methanol and the resulting mixture was heated at reflux temperature for 4.5 h. The solvent was removed under reduced pressure and the residue was froze for 2 h to give cream solids. M.p. = 74.6–75.6 °C. Yield: 2.25 g (80%). Anal. Calcd (%) for $C_{22}H_{22}N_4O_2$ ($M = 374.44 \text{ g mol}^{-1}$): C, 70.57; H, 5.92; N, 14.96. Found: C, 70.68; H, 5.94; N, 14.88. FT-IR bands (KBr, cm^{-1}): $\nu_{\text{C=N}}$ 1651 (s). $^1\text{H NMR}$ (400 MHz, CDCl_3): δ 8.38 (s, 2H, CH=N), 7.32–7.65 (m, 6H, Py- $H_{3,4,5}$), 6.76–7.27 (m, 4H, Ph- $H_{2,4,5,6}$), 4.86 (s, 4H, $-\text{CH}_2-$), 3.97 (s, 3H, Py- OCH_3) ppm. $^{13}\text{C NMR}$ (150 MHz, CDCl_3): δ 163.89, 163.04, 152.10, 139.18, 138.89, 128.78, 127.93, 126.95, 114.28, 112.22, 64.91, 53.42 ppm.

(*E*)-4-phenyl-*N*-((quinolin-2-yl)methylene)aniline (\mathbf{L}^5). Quinoline-2-carboxaldehyde (0.83 g, 5.29 mmol) and 4-phenylaniline (0.90 g, 5.32 mmol) were dissolved in 35 mL of anhydrous methanol and the resulting mixture was heated at reflux temperature for 2 h. The solvent was removed under reduced pressure to give yellow solids. M.p. = 125.1–126.8 °C. Yield: 1.21 g (74%). Anal. Calcd (%) for $C_{22}H_{16}N_2$ ($M = 308.38 \text{ g mol}^{-1}$): C, 85.69; H, 5.23; N, 9.08. Found: C, 85.75; H, 5.28; N, 9.05. FT-IR bands (KBr, cm^{-1}): $\nu_{\text{C=N}}$ 1625 (w). $^1\text{H NMR}$ (400 MHz, CDCl_3): δ 8.91 (s, 1H, CH=N), 8.43 (d, 1H, $J = 5.6 \text{ Hz}$, Quinolone- H_3), 8.31 (d, 1H, $J = 5.6 \text{ Hz}$, Quinolone- H_5), 8.22 (d, 1H, $J = 6.0 \text{ Hz}$, Quinolone- H_2), 8.06 (d, 1H, $J = 6.0 \text{ Hz}$, Quinolone- H_8), 7.94 (t, 1H, $J = 5.6 \text{ Hz}$, Quinolone- H_7), 7.80 (t, 1H, J

= 5.2 Hz, Quinolone- H_6), 7.70 (d, 2H, $J = 5.2 \text{ Hz}$, Ph- $H_{2,6}$), 7.65 (d, 2H, $J = 4.8 \text{ Hz}$, Ph- $H_{3,5}$), 7.53 (d, 2H, $J = 4.8 \text{ Hz}$, *p*-Ph- $H_{2,6}$), 7.47 (t, 2H, $J = 5.6 \text{ Hz}$, *p*-Ph- $H_{3,5}$), 7.37 (t, 1H, $J = 4.8 \text{ Hz}$, *p*-Ph- H_4) ppm. $^{13}\text{C NMR}$ (150 MHz, CDCl_3): δ 160.49, 154.83, 149.82, 147.88, 140.47, 140.06, 136.85, 130.09, 129.65, 128.95, 128.87, 128.02, 127.83, 127.43, 127.02, 121.089, 118.75, 115.41 ppm.

$[\text{ZnL}^1\text{Cl}_2]_2$ ($\mathbf{Zn1}$). To a 5 mL methanol solution of ZnCl_2 (13.3 mg, 0.1 mmol) was slowly added a 25 mL dichloromethane solution of \mathbf{L}^1 (22.7 mg, 0.1 mmol) under stirring. The mixture was stirred and heated under reflux for 8 h. The mixture was then cooled to room temperature and filtered. The filtrate was allowed to stand at room temperature in air. Yellow bulk crystals of $\mathbf{Zn1}$ were obtained by slow evaporation for 21 days. Yield: 21.1 mg (58%). Anal. Calcd (%) for $[\text{C}_{12}\text{H}_9\text{Cl}_2\text{N}_3\text{O}_2\text{Zn}]_2$ ($M = 726.98 \text{ g mol}^{-1}$): C, 39.65; H, 2.50; N, 11.56. Found: C, 39.72; H, 2.61; N, 11.58. FT-IR bands (KBr, cm^{-1}): $\nu_{\text{C=N}}$ 1628(w), $\nu_{\text{Zn-N}}$ 423(w). $^1\text{H NMR}$ (400 MHz, CDCl_3): δ 8.83 (d, $J = 4.8 \text{ Hz}$, 1H, Py- H_6), 8.75 (s, 1H, CH=N), 8.37 (d, $J = 8.4 \text{ Hz}$, 1H, Py- H_3), 8.09 (d, 2H, $J = 8.4 \text{ Hz}$, Ph- $H_{3,5}$), 7.93 (t, 1H, $J = 7.6 \text{ Hz}$, Py- H_4), 7.59 (t, 1H, $J = 5.2 \text{ Hz}$, Py- H_5), 6.64 (d, 2H, $J = 8.8 \text{ Hz}$, Ph- $H_{2,6}$) ppm. $^{13}\text{C NMR}$ (150 MHz, CDCl_3): δ 165.62, 153.56, 148.35, 137.94, 136.86, 130.26, 129.55, 127.12, 123.32, 115.85 ppm.

$[\text{ZnL}^2\text{Cl}_2]$ ($\mathbf{Zn2}$). \mathbf{L}^2 (19.6 mg, 0.1 mmol) and ZnCl_2 (13.6 mg, 0.1 mmol) were refluxed in 20 mL of anhydrous methanol for 4 h. The mixture was then cooled to room temperature and filtered. The filtrate was allowed to stand at room temperature in air. Colorless bulk crystals of $\mathbf{Zn2}$ were obtained by slow evaporation after 29 days. Yield: 21.7 mg (65%). Anal. Calcd (%) for $\text{C}_{13}\text{H}_{12}\text{Cl}_2\text{N}_2\text{Zn}$ ($M = 332.52 \text{ g mol}^{-1}$): C, 46.96; H, 3.64; N, 8.42. Found: C, 47.01; H, 3.57; N, 8.40. FT-IR bands (KBr, cm^{-1}): $\nu_{\text{C=N}}$ 1622(w), $\nu_{\text{Zn-N}}$ 442(w). $^1\text{H NMR}$ (400 MHz, CDCl_3): δ 8.93 (d, 1H, $J = 5.6 \text{ Hz}$, Py- H_6), 8.75 (s, 1H, CH=N), 8.28 (d, 1H, $J = 8.4 \text{ Hz}$, Py- H_3), 7.95 (t, $J = 7.2 \text{ Hz}$, 1H, Py- H_4), 7.40 (t, $J = 6.8 \text{ Hz}$, 1H, Py- H_5), 7.40 (d, 2H, $J = 8.0 \text{ Hz}$, Ph- $H_{2,6}$), 7.02 (d, 2H, $J = 7.6 \text{ Hz}$, Ph- $H_{3,5}$), 2.46 (s, 3H, Ph- CH_3) ppm. $^{13}\text{C NMR}$ (150 MHz, CDCl_3): δ 163.38, 153.72, 151.04, 148.54, 135.36, 133.83, 128.80, 125.49, 122.46, 119.56, 23.17 ppm.

$[\text{Zn}(\mathbf{L}^3)_2] \cdot (\text{ClO}_4)_2$ ($\mathbf{Zn3}$). \mathbf{L}^3 (48.3 mg, 0.2 mmol) and $\text{Zn}(\text{ClO}_4)_2 \cdot 6\text{H}_2\text{O}$ (37.2 mg, 0.1 mmol) were refluxed in 25 mL of anhydrous methanol for 2 h. The mixture was then cooled to room temperature and filtered. The filtrate was allowed to stand at room temperature in air. Yellow bulk crystals of $\mathbf{Zn3}$ were obtained by slow evaporation for 23 days. Yield: 53.9 mg (72%). Anal. Calcd (%) for $\text{C}_{28}\text{H}_{28}\text{Cl}_2\text{N}_4\text{O}_{12}\text{Zn}$ ($M = 748.83 \text{ g mol}^{-1}$): C, 44.91; H, 3.77; N, 7.48. Found: C, 44.88; H, 3.81; N, 7.43. FT-IR bands (KBr, cm^{-1}): $\nu_{\text{C=N}}$ 1619(m), $\nu_{\text{Zn-N}}$ 443(w). $^1\text{H NMR}$ (400 MHz, CDCl_3): δ 8.85 (s, 1H, CH=N), 8.34 (d, 1H, $J = 8.0 \text{ Hz}$, Py- H_5), 8.09 (t, 1H, $J = 8.8 \text{ Hz}$, Py- H_4), 7.78 (d, 1H, $J = 8.4 \text{ Hz}$, Py- H_3), 7.51 (t, 1H, $J = 8.4 \text{ Hz}$, Ph- H_4), 7.45 (d, 1H, $J = 7.2 \text{ Hz}$, Ph- H_6), 7.12 (d, 1H, $J = 6.0 \text{ Hz}$, Ph- H_3), 7.02 (t, 1H, $J = 5.6 \text{ Hz}$, Ph- H_5), 4.25 (s, 3H, Py- OCH_3), 4.18 (s, 3H, Ph- OCH_3) ppm. $^{13}\text{C NMR}$ (150 MHz, CDCl_3): δ 164.51, 153.47, 150.45, 138.56, 128.74, 127.63, 125.44, 122.05, 121.76, 119.25, 117.84, 112.47, 55.82, 54.07 ppm.

$[\text{Zn}_2\mathbf{L}^4\text{Cl}_4]$ ($\mathbf{Zn4}$). \mathbf{L}^4 (37.5 mg, 0.1 mmol) and ZnCl_2 (37.2 mg, 0.2 mmol) were refluxed in 25 mL of anhydrous acetonitrile for 2 h. The

mixture was then cooled to room temperature and filtered. The filtrate was allowed to stand at room temperature in air. Colorless bulk crystals of **Zn4** were obtained by slow evaporation for 6 days. Yield: 43.5 mg (67%). Anal. Calcd (%) for $C_{22}H_{22}Cl_4N_2O_2Zn_2$ ($M = 647.02 \text{ g mol}^{-1}$): C, 40.84; H, 3.43; N, 8.66. Found: C, 40.85; H, 3.47; N, 8.59. FT-IR bands (KBr, cm^{-1}): $\nu_{\text{C=N}}$ 1639(m), $\nu_{\text{Zn-N}}$ 428(w). ^1H NMR (400 MHz, CDCl_3): δ 8.42 (s, 2H, CH=N), 7.70–8.07 (m, 6H, $\text{Py-H}_{3,4,5}$), 6.97–7.52 (m, 4H, $\text{Ph-H}_{2,4,5,6}$), 5.10 (s, 4H, $-\text{CH}_2-$), 4.04 (s, 3H, Py-OCH_3) ppm. ^{13}C NMR (150 MHz, CDCl_3): δ 163.97, 162.10, 150.72, 140.19, 134.47, 129.31, 128.93, 126.41, 116.52, 115.54, 63.75, 54.48 ppm.

$[\text{ZnL}^5\text{Cl}_2]$ (**Zn5**). L^5 (31.0 mg, 0.1 mmol) and ZnCl_2 (13.6 mg, 0.1 mmol) were refluxed in 25 mL of anhydrous acetonitrile for 2 h. The mixture was then cooled to room temperature and filtered. The filtrate was allowed to stand at room temperature in air. Yellow bulk crystals of **Zn5** were obtained by slow evaporation for 3 days. Yield: 26.3 mg (59%). Anal. Calcd (%) for $C_{22}H_{16}Cl_2N_2Zn$ ($M = 444.64 \text{ g mol}^{-1}$): C, 59.43; H, 3.63; N, 6.30. Found: C, 59.37; H, 3.66; N, 6.25. FT-IR bands (KBr, cm^{-1}): $\nu_{\text{C=N}}$ 1621(w), $\nu_{\text{Zn-N}}$ 428(w). ^1H NMR (400 MHz, CDCl_3): δ 9.01 (s, 1H, CH=N), 8.73 (d, 1H, $J = 8.8 \text{ Hz}$, Quinolone- H_3), 8.67 (d, 1H, $J = 8.4 \text{ Hz}$, Quinolone- H_5), 8.47 (d, 1H, $J = 7.6 \text{ Hz}$, Quinolone- H_2), 8.10 (d, 1H, $J = 5.6 \text{ Hz}$, Quinolone- H_8), 8.04 (t, 1H, $J = 7.6 \text{ Hz}$, Quinolone- H_7), 7.97 (t, 1H, $J = 8.8 \text{ Hz}$, Quinolone- H_6), 7.87 (d, 2H, $J = 8.0 \text{ Hz}$, $\text{Ph-H}_{2,6}$), 7.77 (d, 2H, $J = 8.4 \text{ Hz}$, $\text{Ph-H}_{3,5}$), 7.64 (d, 2H, $J = 7.2 \text{ Hz}$, $p\text{-Ph-H}_{2,6}$), 7.52 (t, 2H, $J = 8.8 \text{ Hz}$, $p\text{-Ph-H}_{3,5}$), 7.45 (t, 1H, $J = 6.4 \text{ Hz}$, $p\text{-Ph-H}_4$) ppm. ^{13}C NMR (150 MHz, CDCl_3): δ 161.45, 150.59, 147.90, 145.11, 139.79, 139.14, 133.69, 130.16, 129.99, 129.17, 128.58, 127.15, 127.04, 126.64, 126.49, 124.12, 117.06, 115.76 ppm.

Fabrication of complex Zn3–PMMA films

PMMA was doped with complex **Zn3** in proportions of 0.25%, 0.5%, 0.75%, 1.0%, 2.0%, 4.0% and 6.0%. The PMMA powder was dissolved in N,N' -dimethylformamide (DMF), followed by addition of the required of complex **Zn3** in DMF solution and the resulting mixture was heated at 50 °C for 60 min. The polymer film was obtained after the total evaporation of excess solvent at 60 °C according to the literatures.

Results and Discussion

Synthesis and spectral characterization

The structures of five Schiff base ligands ($\text{L}^1\text{--L}^5$) are shown in Scheme 1. Yields for these ligands varied from 67 to 90%. Using a self-assembled method, these ligands were reacted with $\text{ZnCl}_2/\text{Zn}(\text{ClO}_4)_2$ to obtain a series of complexes, namely, **Zn1–Zn5**. X-ray quality single crystals of five Zn(II) complexes were grown from slow evaporation of solutions and readily obtained in good yields within the range of 58–72%. The details of the synthesis are given in the experimental section. Some important analytical and physical data are listed in Table S3†. The composition of the ligands and complexes were calculated and compared with the experimental values. We confirm that all the complexes are stable in the solid state under exposure to air. The complexes are soluble in common organic solvents, such as chloroform, dimethylsulfoxide and acetonitrile.

The infrared spectra of these five Zn(II) complexes (see Figs S1–S5†) are similar to that of the corresponding ligand and the IR assignments of selected diagnostic bands are given in the experimental section. In the IR spectra of ligands $\text{L}^1\text{--L}^5$, the existence of C=N bonds is clearly demonstrated by the presence of strong characteristic C=N peaks in a range of 1628–1651 cm^{-1} . These bands undergo negative shifts of 2–13 cm^{-1} in the complexes, which may be attributed to the coordination of the nitrogen atom of the imine to the metal ion.^{41,42} This is further confirmed by the presence of a $\nu(\text{M–N})$ vibration in the region 423–443 cm^{-1} in all the complexes.⁴³ The ^1H NMR spectra of the ligands $\text{L}^1\text{--L}^5$ and its Zn(II) complexes were recorded in CDCl_3 at room temperature (see Figs S6–S10†). In the ^1H NMR spectra, the chemical shift values of the protons in the complexes are slightly different from those observed for the non-coordinated ligand. Of particular note is the HC=N resonances of the complexes **Zn1–Zn5**, which are moved downfield due to coordination between the imine nitrogen and the Zn(II) center.⁴⁴ For the complexes, the imine proton is moved downfield at most 0.04 ppm. In the ^{13}C NMR spectra (see Figs S11–S15†), the signals of the C=N nuclei are observed at δ 159.63–165.62 ppm.

We performed powder X-ray diffraction patterns on complexes **Zn1–Zn5** to check the purity of the bulk products. From Fig S16†, we can see that all major peak positions of the measured patterns are in good agreement with those simulated. Furthermore, the differences in intensity may be due to the preferred orientation of the crystal products. To further understand the structures of these complexes, single crystals were obtained and analyzed by Single Crystal X-ray Diffraction. The crystallographic data for these complexes **Zn1–Zn5** are listed in Table 1.

Description of the structures

$[\text{ZnL}^1\text{Cl}_2]$ (**Zn1**). Complex **Zn1** crystallized in the monoclinic space group $P2_1/c$. As shown in Fig. 1a, the asymmetric unit of **Zn1** consists of one Zn(II) atom, one L^1 ligand and two chlorine anions. Using Addison's model,^{45,46} the coordination geometry around the zinc atom in **Zn1** ($\tau_4 = 0.772$) can be better described as a tetrahedron. It is noteworthy that it gives rise to a five-membered ring after coordinated, which have coplanar with inherency of pyridyl ring and indirectly results the extended conjugate. In complex **Zn1**, the pyridine ring and the phenyl rings of L^1 ligand are twisty and the dihedral angle is $\sim 29.301^\circ$. The average bond lengths of Zn–N and Zn–Cl are 2.145(2) and 2.281(7) Å, respectively. The bond angles around the Zn(II) ion are in the range of 77.84(6)–132.87(5)°. The selected bond lengths and bond angles of complex **Zn1** are given in Table S1†. Single crystal analysis shows that complex **Zn1** is constructed by the C–H \cdots O and C–H \cdots Cl hydrogen bonds interactions⁴⁷ and $\pi\cdots\pi$ stacking interactions to aggregate in a three-dimensional supramolecular network (Fig. 1b). The $\pi_{\text{phenyl}}\cdots\pi_{\text{phenyl}}$ and $\pi_{\text{phenyl}}\cdots\pi_{\text{pyridyl}}$ distances are 3.561 and 3.802 Å, respectively. The detailed data of C–H \cdots O/Cl hydrogen bonds and $\pi\cdots\pi$ interactions for **Zn1** are listed in Table 2. If the mononuclear unit is viewed as the nodes, the C–H \cdots O/Cl and $\pi\cdots\pi$ interactions as the linkers, the resulting three-dimensional supramolecular structure may be simplified as a *pcu* net with the point symbol of $\{4^{12}\cdot 6^3\}$, as depicted in Fig. 1c.

Table 1. Crystallographic and structural determination data for complexes Zn1–Zn5.

	Zn1	Zn2	Zn3	Zn4	Zn5
CCDC No.	1508968	1508969	1508970	1508971	1508972
formula	[C ₁₂ H ₉ Cl ₂ N ₃ O ₂ Zn] ₂	C ₁₃ H ₁₂ Cl ₂ N ₂ Zn	C ₂₈ H ₂₈ Cl ₂ N ₄ O ₁₂ Zn	C ₂₂ H ₂₂ Cl ₄ N ₂ O ₂ Zn ₂	C ₂₂ H ₁₆ Cl ₂ N ₂ Zn
<i>M_r</i>	726.98	332.52	748.83	647.02	444.64
cryst syst	Monoclinic	Monoclinic	Triclinic	Triclinic	Triclinic
space group	<i>P</i> 2 ₁ / <i>c</i>	<i>P</i> 2 ₁ / <i>c</i>	<i>P</i> $\bar{1}$	<i>P</i> 2 ₁ / <i>c</i>	<i>P</i> $\bar{1}$
<i>a</i> [Å]	9.401(19)	11.952(7)	8.441(5)	15.062(2)	8.473(5)
<i>b</i> [Å]	7.409(15)	9.847(8)	10.097(8)	12.753(19)	9.740(5)
<i>c</i> [Å]	20.197(4)	14.876(6)	19.157(13)	15.887(2)	12.535(6)
α [°]	90	90	103.765(2)	90	82.088(4)
β [°]	98.51(3)	127.535(19)	94.754(2)	118.539(11)	72.926(5)
γ [°]	90	90	101.537(2)	90	78.764(5)
Volume [Å ³]	1391.3(5)	1388.33(15)	1539.29(18)	2680.9(6)	966.44(9)
<i>Z</i>	2	4	2	4	2
<i>D_c</i> [g cm ⁻³]	1.735	1.591	1.616	1.603	1.528
μ [mm ⁻¹]	2.152	2.136	1.043	2.215	1.556
<i>F</i> (000)	728	672	768	1304	452
Θ range [°]	3.21–27.45	3.43–27.48	3.01–25.00	3.02–25.36	3.03–25.00
<i>h</i> range	–11 ≤ <i>h</i> ≤ 12	–15 ≤ <i>h</i> ≤ 15	–10 ≤ <i>h</i> ≤ 10	–17 ≤ <i>h</i> ≤ 17	–10 ≤ <i>h</i> ≤ 10
<i>k</i> range	–9 ≤ <i>k</i> ≤ 9	–12 ≤ <i>k</i> ≤ 12	–12 ≤ <i>k</i> ≤ 11	–15 ≤ <i>k</i> ≤ 15	–11 ≤ <i>k</i> ≤ 11
<i>l</i> range	–26 ≤ <i>l</i> ≤ 26	–17 ≤ <i>l</i> ≤ 19	–22 ≤ <i>l</i> ≤ 22	–17 ≤ <i>l</i> ≤ 19	–14 ≤ <i>l</i> ≤ 11
data/restraints/params	3176 / 0 / 181	3160 / 0 / 163	5330 / 0 / 424	4857 / 0 / 307	3398 / 0 / 244
GOF	1.017	1.065	1.073	0.795	0.917
<i>R_i</i> , <i>wR</i> ₂ [I > 2σ(I)] ^a	0.0283, 0.0662	0.0635, 0.1528	0.0731, 0.1935	0.0480, 0.1166	0.0505, 0.0775
<i>R_i</i> , <i>wR</i> ₂ [all data] ^a	0.0360, 0.0688	0.1134, 0.1771	0.1175, 0.2164	0.1450, 0.2162	0.0884, 0.0882
$\Delta\rho_{\max}$, $\Delta\rho_{\min}$ [e ⁻ Å ⁻³]	0.319, –0.300	1.383, –0.492	1.748, –0.700	0.495, –0.306	0.361, –0.496

^a $R_1 = \sum ||F_o| - |F_c|| / \sum |F_o|$; $wR_2 = [\sum [w(F_o^2 - F_c^2)^2] / \sum [w(F_o^2)^2]]^{1/2}$.

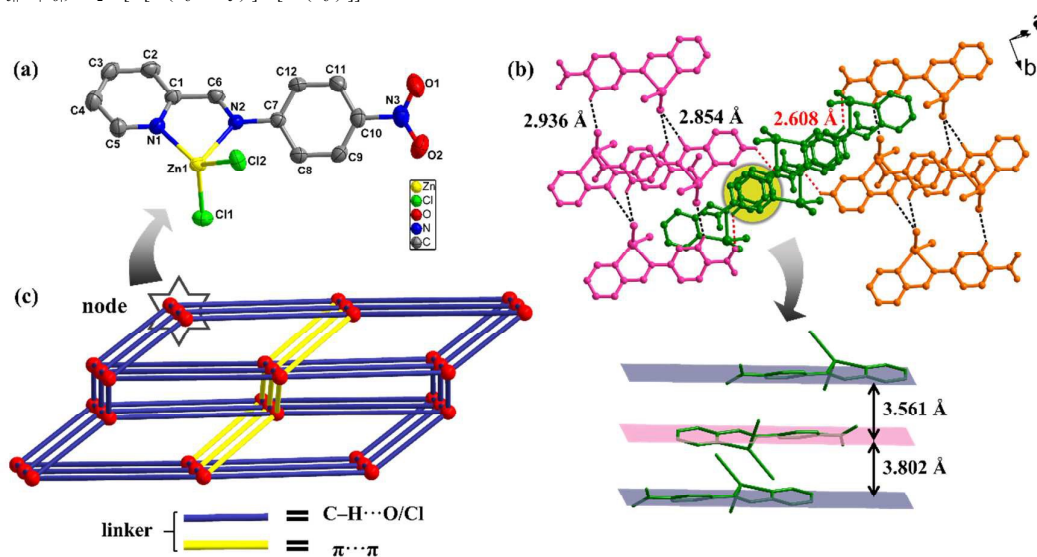


Fig. 1 (a) Crystal structure of Zn1. Thermal ellipsoid is drawn at 50% probability. H atoms have been omitted for clarity. (b) The 3D network structure in Zn1. (c) The 3D six-connected network with *pcu* topology and point symbol {4¹²-6³} of Zn1. Dotted lines represent the C–H···O and C–H···Cl interactions.

[ZnL²Cl₂] (Zn2). Crystal refinement data of complex Zn2 implied that it belongs to a monoclinic system, *P*2₁/*c* space group. As shown in Fig. S17a†, the Zn(II) center adopts a distorted tetrahedral geometry ($\tau_4 = 0.888$) coordinated by two nitrogen atoms of (*E*)-4-methyl-*N*-((pyridin-2-yl)methylene)aniline (L²) and two terminal chlorine ions (Zn1–N1 = 2.054(5) Å, Zn1–N2 = 2.092(5) Å, Zn1–Cl1 = 2.203(2) Å, Zn1–Cl2 = 2.194(2) Å). The bond angles for Zn(II) are in the range of 80.6(2)–125.0(4)°. The dihedral angle between the pyridyl ring and the phenyl ring is 7.177° (Table 2), which is close to parallel. In the *bc* plane, the independent units are linked through C3–H3A···Cl1 hydrogen bonds interactions (the

distance of H3A···Cl1 is 2.929 Å, and the C3–H3A···Cl1 angle is 161.099°) to generate a one-dimensional chain (Fig. 2a). In addition, the molecules are also interconnected by C5–H5A···Cl2, C6–H6A···Cl1 and C8–H8A···Cl2 hydrogen bonds interactions (the distances of H5A···Cl2, H6A···Cl1 and H8A···Cl2 are 2.860, 2.895 and 2.945 Å, respectively) to aggregate in a two-dimensional layer (Fig. 2b), and the π ··· π stacking interactions with centroid···centroid distances of 3.662 and 3.872 Å exist in the sheet (Fig. S17b†). These 1D and 2D structures are both constructed to the resulting 3D supramolecular

ARTICLE

Journal Name

structure of **Zn2** (Fig. 2c). Topology analysis shows that the overall network of **Zn2** features a 3D *pcu* topology with a point symbol of $\{4^{12}\cdot6^3\}$ by denoting the mononuclear unit as 6-connected nodes and the C–H \cdots Cl interactions as linkers, respectively.

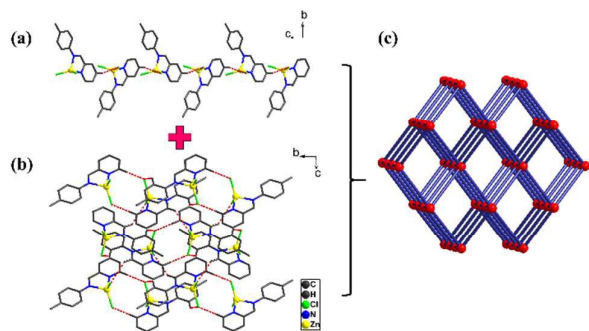


Fig. 2 (a) The 1D chain structure in **Zn2**. (b) The 2D layer structure in **Zn2**. (c) The 3D six-connected network with *pcu* topology and point symbol $\{4^{12}\cdot6^3\}$ of **Zn2**. Dotted lines represent the C–H \cdots Cl interactions.

[Zn(L³)₂](ClO₄)₂ (Zn3**)**. The asymmetric unit of complex **Zn3** consists of one crystallographically independent Zn²⁺ cation, two L³ ligands, and two ClO₄[−] anions (Fig. 3a). Every Zn²⁺ cation is six-coordinated with slightly distorted octahedral coordination geometry [ZnN₄O₂] containing four N atoms (N1, N2, N3 and N4) and two O atoms (O2 and O4) from L³ (Fig. 3b). The bond angles around the Zn(II) ion are in the range of 70.3(2)–152.17(19) Å. The selected bond distances and angles are shown in Table S2†. In complex **Zn3**, the dihedral angles (88.765°) between two L³ ligands is approximately perpendicular (Fig. 3c). In the molecular packing structure of complex **Zn3**, the intramolecular hydrogen bonds

interactions (C7–H7D \cdots O6 and C13–H13A \cdots O11) based on the O atom of ClO₄[−] anion are found (Fig. 3d). Besides these, the intermolecular hydrogen bonds interactions play important roles in forming the higher dimensional structure. As shown in Fig. 3d, the adjacent molecules are linked by C7–H7B \cdots O5, C7–H7C \cdots O8, C11–H11B \cdots O12 and C28–H28B \cdots O11 hydrogen bonds interactions to form a 3D supramolecular structure. The distances of H7B \cdots O5, H7C \cdots O8, H11B \cdots O12 and H28B \cdots O11 are 2.543, 2.570, 2.698 and 2.358 Å, respectively. Finally, the overall topology of **Zn3** can also be defined as the $\{4^{12}\cdot6^3\}$ topology as illustrated in Fig. 3e.

[Zn₂L⁴Cl₄] (Zn4**)**. The asymmetric unit of complex **Zn4** consists of two crystallographically independent Zn²⁺ cations, one ligand L⁴, and four Cl[−] anions (Fig. 4a). The lengths and angles of center ion coordination bond (see Table S2†) have small differences. In complex **Zn4**, the zinc(II) ions are four-coordinated, and the coordination geometry of Zn²⁺ are distorted tetrahedron (Fig. 4b), with geometry index $\tau_4 = 0.883$ (Zn1) and 0.863 (Zn2). In the binuclear structure unit, intermetallic Zn(1) \cdots Zn(2) distance is 8.362(11) Å. Due to the flexibility of –CH₂– group, the pyridyl and phenyl rings of the L⁴ ligand in **Zn4** are arranged in a nearly perpendicular fashion (77.840°/80.059°). The adjacent binuclear molecules are interconnected through C6–H6A \cdots Cl4, C7–H7B \cdots Cl4, C10–H10A \cdots Cl3, and C13–H13A \cdots Cl1 hydrogen bonds interactions to form a 3D supramolecular structure (Fig. 4c). The H6A \cdots Cl4, H7B \cdots Cl4, H10A \cdots Cl3, and H13A \cdots Cl1 distances are 2.626, 2.813, 2.922 and 2.612 Å, respectively. From the topological point of view, the binuclear unit could be considered as the node, and hydrogen bonds C–H \cdots Cl could be considered as the linkers. Thus, the three-dimensional net of **Zn4** can be described as a 7-connected with the point symbol of $\{4^{17}\cdot6^4\}$ (Fig. 4d).

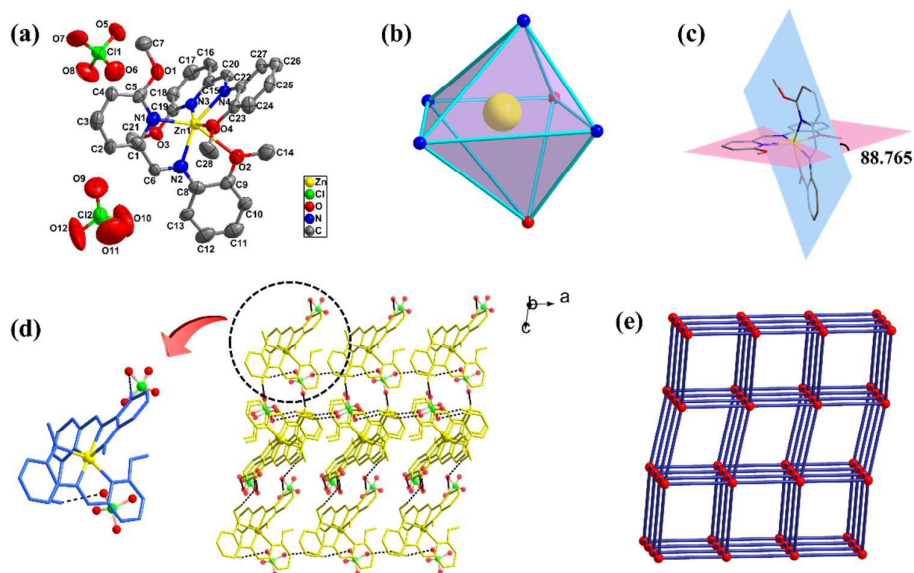


Fig. 3 (a) Crystal structure of **Zn3**. Thermal ellipsoid is drawn at 50% probability. H atoms have been omitted for clarity. (b) Coordination geometry of zinc(II) ions. (c) Depiction of the dihedral angle between two L³ ligands. (d) The 3D network structure in **Zn3**. (e) The 3D six-connected network with *pcu* topology and point symbol $\{4^{12}\cdot6^3\}$ of **Zn3**. Dotted lines represent the C–H \cdots O interactions.

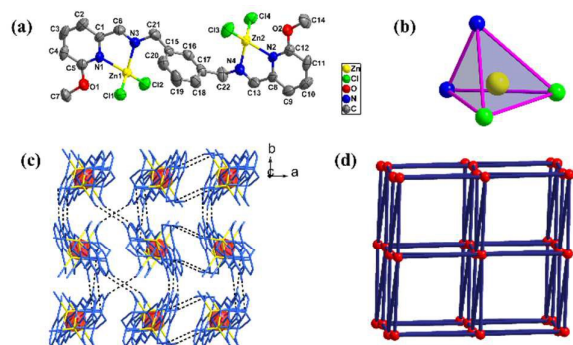


Fig. 4 (a) Crystal structure of **Zn4**. Thermal ellipsoid is drawn at 50% probability. H atoms have been omitted for clarity. (b) Coordination geometry of zinc(II) ions. (c) The 3D network structure in **Zn4**. (d) The 3D seven-connected network and point symbol $\{4^{17} \cdot 6^4\}$ of **Zn4**. Dotted lines represent the C–H \cdots Cl interactions.

[ZnL⁵Cl₂] (Zn5). The single-crystal X-ray diffraction analysis reveals that complex **Zn5** crystallizes in the triclinic system, space group *P*1 with one molecule of the complex in the unit cell. As shown in Fig. 5a, the coordination number of Zn(II) is four ($\tau_4 = 0.888$) with two nitrogen atoms from ligand **L⁵** and two terminal chlorine atoms. Complex **Zn5** has the dihedral angles of 10.161°, between quinoline ring and phenyl ring, which indicate that **Zn5** displays better coplanarity. The distances of Zn1–N1 and Zn1–N2 are 2.070(3) Å and 2.093(3) Å, in agreement with the values of a similar zinc complex.⁴⁸ The distance of Zn1–Cl2 (2.215(12) Å) is longer than that of Zn1–Cl1 (2.177(11) Å). The detailed bond

distances and angles are listed in Table S2†. In complex **Zn5**, the independent units are linked through hydrogen bonds C10–H10A \cdots Cl2 of 2.851 Å, C12–H12A \cdots Cl2 of 2.872 Å and C18–H18A \cdots Cl1 of 2.947 Å interactions respectively, to generate a one-dimensional “wave-like” chains (Fig. 5b). Significantly, additional intermolecular $\pi\cdots\pi$ interactions with separations of about 3.657 Å (Fig. 5b) also provide further stabilization in the complex **Zn5**. The detailed data of the noncovalent bond interactions (C–H \cdots O/Cl and $\pi\cdots\pi$) for all complexes are listed in Table 2.

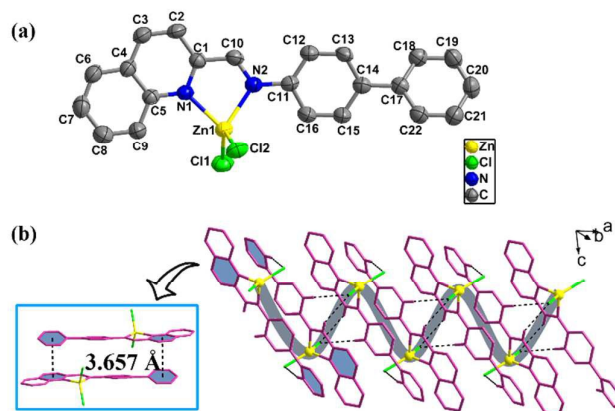


Fig. 5 (a) Crystal structure of **Zn5**. Thermal ellipsoid is drawn at 50% probability. H atoms have been omitted for clarity. (b) The 1D “wave-like” chain structure in **Zn5**. Dotted lines represent the C–H \cdots Cl and $\pi\cdots\pi$ interactions.

Table 2. Structural and geometrical parameters for complexes **Zn1–Zn5**.

Complex	Addison parameter (τ_4)	Dihedral angle (deg) ^d	D–H \cdots A	D–H (Å)	H \cdots A (Å)	D \cdots A (Å)	D–H \cdots A (deg)	Dimension
Zn1	0.772	29.301	C4–H4A \cdots O2	0.930	2.608	3.291	130.684(1)	3D
			C6–H6A \cdots Cl1	0.930	2.854	3.777	171.515(9)	
			C9–H9A \cdots Cl1	0.930	2.936	3.663	136.002(1)	
			$\pi_{C_{61}}\cdots\pi_{C_{61}}$ ^c			3.561		
			$\pi_{C_{61}}\cdots\pi_{C_{62}}$ ^d			3.802		
Zn2	0.888	7.177	C3–H3A \cdots Cl1	0.950	2.929	3.840	161.099(3)	3D
			C5–H5A \cdots Cl2	0.950	2.860	3.554	133.958	
			C6–H6A \cdots Cl1	0.950	2.895	3.610	132.987(3)	
			C8–H8A \cdots Cl2	0.950	2.945	3.614	128.480(4)	
			$\pi_{C_{61}}\cdots\pi_{C_{62}}$			3.662, 3.872		
Zn3	—	20.087, 1.924	C7–H7B \cdots O5	0.980	2.543	3.442	152.544(5)	3D
			C7–H7C \cdots O8	0.980	2.570	3.489	156.181(5)	
			C7–H7D \cdots O6	0.980	2.692	3.495	139.420(5)	
			C11–H11B \cdots O12	0.950	2.698	3.416	132.923(6)	
			C13–H13A \cdots O11	0.950	2.600	3.550	178.479(6)	
			C28–H28B \cdots O11	0.980	2.358	3.326	169.181(5)	
			$\pi_{C_{61}}\cdots\pi_{C_{62}}$			3.715		
			$\pi_{C_{62}}\cdots\pi_{C_{63}}$ ^e					
Zn4	0.883, 0.863	77.840, 80.059	C6–H6A \cdots Cl4	0.930	2.626	3.527	163.285(7)	3D
			C7–H7B \cdots Cl4	0.960	2.813	3.739	16.261(1)	
			C10–H10A \cdots Cl3	0.930	2.922	3.569	127.918(1)	
			C13–H13A \cdots Cl1	0.930	2.612	3.534	171.299(7)	
			$\pi_{C_{62}}\cdots\pi_{C_{63}}$ ^e			3.657		
Zn5	0.888	10.161 ^b	C10–H10A \cdots Cl2	0.930	2.851	3.607	139.221(5)	1D
			C12–H12A \cdots Cl2	0.930	2.872	3.754	158.769(7)	
			C18–H18A \cdots Cl1	0.930	2.947	3.861	167.708(8)	
			$\pi_{C_{62}}\cdots\pi_{C_{63}}$ ^e			3.657		
			$\pi_{C_{62}}\cdots\pi_{C_{63}}$ ^e			3.657		

^a Between the pyridyl ring and phenyl ring; ^b Between the quinoline ring and phenyl ring; ^c C_{61} = phenyl ring; ^d C_{62} = pyridyl ring; ^e C_{63} = quinoline ring.

ARTICLE

Photophysical Studies. *Absorption Properties of the Zinc(II) Complexes in CH₃CN.* The UV-vis absorption spectra of the ligands **L¹–L⁵** and complexes **Zn1–Zn5** were recorded at room temperature in CH₃CN (10 μmol L⁻¹). Fig. 6 shows the absorption spectra of complexes **Zn1–Zn5** in acetonitrile. It is found that all the complexes exhibit two distinct absorption bands at *ca.* 280 nm and *ca.* 350 nm. The numerical values of the maximum absorption wavelength and molar extinction coefficients (ϵ) are listed in Table 3. For complexes **Zn1–Zn5**, these absorption bands are similar to the corresponding ligands (Fig. S18†) which can be assigned to the π – π^* transitions of the ligands.⁴⁹ The low energy absorption bands of complexes **Zn2–Zn5** were 341, 375, 340, 374 nm, respectively, which shifted to longer wavelengths compared to that of **Zn1** (330 nm) due to the increase of electron-donating groups and conjugated system.

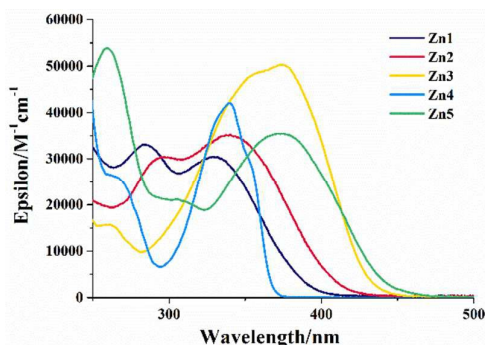


Fig. 6 UV-vis absorption spectra of **Zn1–Zn5** in CH₃CN at room temperature.

Solid-State and Solution Luminescence Properties of the Zinc(II) Complexes. Luminescent zinc(II) complexes possessing closed d¹⁰ shells are superior potential candidates as valuable luminescent materials;^{50–52} thus, we probed the luminescence properties of **Zn1–Zn5** in the solid state and acetonitrile solution at room temperature. Selected data are summarized in Table 3. In the solid state, the free ligands **L¹–L⁵** exhibit emission bands from blue to green centered at 446, 474, 521, 472, and 531 nm (Fig. S19a† and S19b†), respectively, which may be attributed to the π^* – π transitions.^{53,54} For the complexes **Zn1–Zn5**, the emission bands are observed at 461, 483, 532, 514, and 592 nm (Fig. 7a and 7b), respectively. Due to the similarity of the emission bands with that of the corresponding ligand, the emissions of these zinc(II) complexes may be attributed to the intraligand transitions.^{55,56} In addition, the emission bands of **Zn1–Zn5** occur red-shifted compared to that of the corresponding ligand, which may be attributed to the coordination of ligand to the metal centers. A trend is observed in λ_{em} with **Zn1** < **Zn2** < **Zn4** < **Zn3** < **Zn5** which is consistent with the electron-donating ability (–NO₂ < –CH₃ < –OCH₃) of substituents and conjugated system of these ligands **L¹–L⁵**. Electron-donating effect descended the energy difference between HOMO and LUMO, leading to λ_{em} red shifted.⁵⁷

In acetonitrile solution, the emission bands are observed at 390–465 nm and 415–560 nm for ligands **L¹–L⁵** (Fig. S19c† and S19d†) and complexes **Zn1–Zn5** (Fig. 7c and 7d), respectively. The Commission Internationale d’Eclairage (CIE) coordinates are summarized in Table 3. In acetonitrile solution, the maxima emission peaks are blue-shifted 18–100 nm compared with those in the solid state. These phenomena can be explained due to the less

polar nature in the solid-state environment (in addition to the specific interactions at the solid state). We also drawn the corresponding emission energy spectra of the ligands and complexes (Fig. S20†) and summarized the emission energy data in the Table S4†. In acetonitrile solution, the maxima emission energies shift 0.08–0.57 eV compared with those in the solid state. Among the complexes, **Zn2** shows the largest shift (0.42 eV). Meanwhile, the full width at half-maximum (FWHM) of the emission band decreases from acetonitrile solution to the solid state (Table 3). All luminescence quantum yields of complexes **Zn1–Zn5** in solution were measured by the optical dilute method of Demas and Crosby⁵⁸ with a standard of quinine sulfate ($\Phi_F = 0.546$) and are listed in Table 3. The luminescence quantum yield of **Zn1–Zn5** in CH₃CN is 0.015, 0.106, 0.533, 0.149 and 0.228, respectively, which is higher than that of the corresponding ligand. Particularly, the quantum yields of **Zn3** ($\Phi_F = 0.533$) is *ca.* 11-fold to **L³** ($\Phi_F = 0.048$). This is because the ligands coordinated with zinc(II) ions increase the rigidity of the molecular edifice and reduce the loss of energy by radiationless thermal vibrations.⁵⁹

The luminescence decay profiles of ligands **L¹–L⁵** and the corresponding zinc(II) complexes were measured at their optimal excitation wavelengths in the solid state and acetonitrile solution at 298 K. The detailed data are listed in Table S5†. A general trend is that the luminescence lifetimes for complexes **Zn1–Zn5** either in the solid state or acetonitrile solution at 298 K is longer than that of the corresponding ligands **L¹–L⁵**. The most obvious observation is that the lifetime of **Zn1** ($\tau = 7.60$ μs) is 1.6-fold to the corresponding ligand **L¹** ($\tau = 4.75$ μs) in acetonitrile solution. This is attributed to the more stable structure and interaction upon coordination.⁶⁰ Meanwhile, the luminescence lifetimes of the ligand and corresponding complexes in the solid state ($\tau = 7.71$ –13.06 μs for **L¹–L⁵**; $\tau = 7.90$ –14.58 μs for **Zn1–Zn5**) are longer than those in acetonitrile solution ($\tau = 4.75$ –7.48 μs for **L¹–L⁵**; $\tau = 7.60$ –8.78 μs for **Zn1–Zn5**), which might be attributed to their less polar nature in the solid-state environment.⁶¹

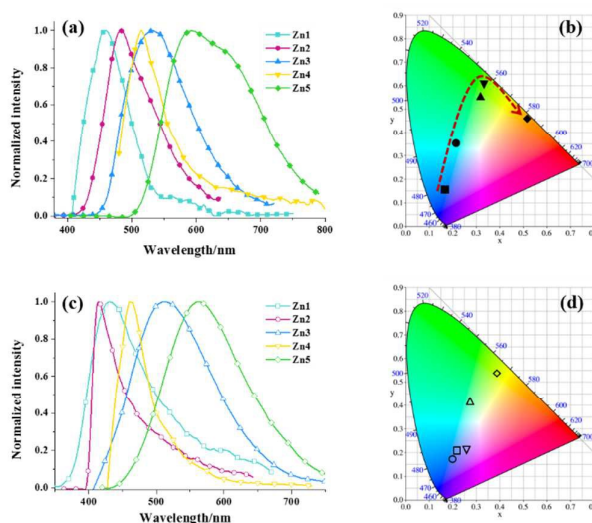


Fig. 7 (a) Emission spectra of **Zn1–Zn5** in the solid state and (b) CIE chromaticity diagram (1931 CIE standard). (c) Emission spectra of **Zn1–Zn5** in acetonitrile solution and (d) CIE chromaticity diagram.

Table 3. Photophysical properties of the ligands L^1 – L^5 and complexes **Zn1**–**Zn5**.

Complex	absorption ^a	photoluminescence in acetonitrile					photoluminescence in the solid state			
	$\lambda_{\text{abs}}/\text{nm}$ ($\epsilon/\text{M}^{-1}\text{cm}^{-1}$)	$\lambda_{\text{em}}/\text{nm}$	FWHM/nm	$\tau/\mu\text{s}$	Φ_{PL}^b	CIE (x, y)	$\lambda_{\text{em}}/\text{nm}$	FWHM/nm	$\tau/\mu\text{s}$	CIE (x, y)
L ¹	275 (16172), 320 (20061)	390	97.05	4.75	0.009	0.16, 0.17	446	151.28	7.80	0.21, 0.22
Zn1	285 (33040), 330 (30370)	430	86.51	7.60	0.015	0.22, 0.20	461	69.15	7.90	0.16, 0.15
L ²	283 (26774), 323 (21417)	410	84.18	5.58	0.017	0.16, 0.07	474	101.71	7.71	0.18, 0.24
Zn2	295 (30540), 341 (35185)	415	45.81	7.95	0.106	0.20, 0.18	483	92.97	9.41	0.21, 0.36
L ³	308 (34392), 354 (20004)	421	102.45	5.22	0.048	0.23, 0.21	521	188.23	13.06	0.30, 0.39
Zn3	261 (15695), 375 (50244)	514	134.77	8.78	0.533	0.29, 0.42	532	111.02	14.58	0.35, 0.54
L ⁴	271 (21679), 325 (29229)	430	64.37	7.48	0.037	0.18, 0.14	472	101.84	7.98	0.16, 0.26
Zn4	267 (25871), 340 (42044)	460	53.06	8.02	0.149	0.17, 0.19	514	76.12	10.06	0.30, 0.59
L ⁵	265 (36606), 346 (27063)	465	73.28	6.67	0.055	0.22, 0.20	531	100.90	8.03	0.38, 0.56
Zn5	261 (53841), 374 (35464)	560	135.94	8.50	0.228	0.43, 0.51	592	163.72	9.38	0.54, 0.46

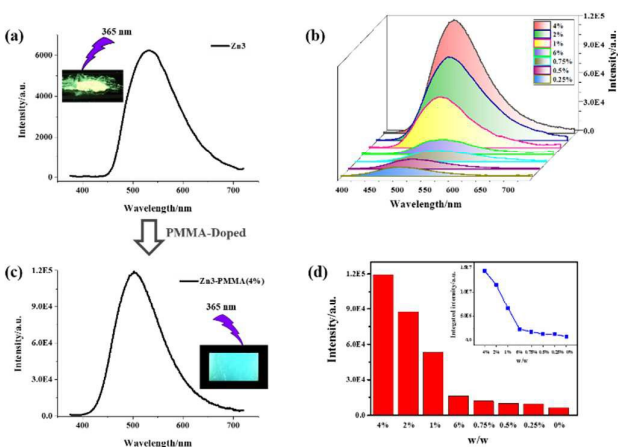
^a Measured in CH_3CN solutions ($\sim 1 \times 10^{-5}$ M). ^b Take quinine sulfate in CH_3CN as reference ($\sim 1 \times 10^{-5}$ M, $\Phi_{\text{PL}} = 0.546$).

Properties of PMMA polymer films doped with complex **Zn3**.

Based on the naked-eye visible bright luminescence of complex **Zn3** (Fig. 8a), considering the good performance of PMMA as one of the most popular polymer matrices with low cost, easy preparation, and good mechanical properties, a new PMMA-supported hybrid film material is constructed by doping complex **Zn3** into PMMA polymer.

To better illustrate the intra structure of PMMA-supported film, FT-IR spectra of pure PMMA, complex **Zn3**, **Zn3**-PMMA are recorded, as shown in Fig. S21†. The band at 1732 cm^{-1} for pure PMMA is ascribed to the C=O vibrating absorption of PMMA, but when doped with complex **Zn3**, the band of C=O vibrating absorption shifts to 1726 cm^{-1} . This implies that there exist intermolecular interaction between complex **Zn3** and PMMA.⁶²

As an extension of this work, we study the luminescence properties of the newly designed hybrid film material. The emission spectra of the PMMA polymer films doped with complex **Zn3** at different concentrations [0.25%, 0.5%, 0.75%, 1.0%, 2.0%, 4.0% and 6.0% (w/w)] are similar with maximum excitation peak at 365 nm (Fig. 8b). The emission bands are assigned to the $\pi^*-\pi$ transitions of ligand **L**³. Noticeably, the luminescence intensity of the maximum emission increases with the increasing concentration of complex **Zn3** from 0.25% to 4.0%, and begin to decrease when doping concentration surpasses 4.0%. It can be attributed to the fact that with a low concentration of complex **Zn3** in the PMMA polymer, the complex **Zn3** can disperse uniformly in the PMMA matrix and the PMMA effectively enhance the luminescence behavior of the complex **Zn3**. Upon further increasing concentration of complex **Zn3** after 4.0%, some aggregates formed in the film and the transparency of films declines, influencing the absorption of light, resulting in intensity decrease of luminescence, which means luminescence quenching of complex **Zn3**. Comparing the emission spectra of **Zn3** (Fig. 8a) and **Zn3**-PMMA (Fig. 8c), the luminescence intensity and integrated intensity of **Zn3**-PMMA is much higher than **Zn3** (Fig. 8d). Furthermore, the luminescence intensity of the PMMA polymer film with best doping concentration at 4.0% reached 19 times of complex **Zn3**. TG analysis of **Zn3**-PMMA films shows no weight-loss in the temperature range of 25–278 °C (Fig. S22†), revealing a significant increase of 98 °C in comparison with **Zn3**, which suggests that the thermal stability of



the **Zn3**-PMMA films is essentially improved by doping with complex **Zn3**.

Fig. 8 (a) Emission spectrum and photo of complex **Zn3** under UV light with 365 nm in the solid state. (b) Emission spectra of **Zn3**-PMMA films doped with 0.25%–6% of **Zn3**. (c) Emission spectrum and photo of **Zn3**-PMMA at 4% concentration under UV light with 365 nm. (d) Comparison of the intensity and integrated intensity of **Zn3**-PMMA films doped with 0–6% of **Zn3**.

Conclusions

In summary, five Zn(II) complexes with different conjugated system were synthesized. Based on these five complexes different supramolecular structures were constructed *via* different intermolecular weaker interactions such as hydrogen bonding C–H \cdots O/Cl and $\pi\cdots\pi$ packing interactions, which are a three-dimensional $\{4^{12}\cdot 6^3\}$ topology for **Zn1**–**Zn3**, a three-dimensional $\{4^{17}\cdot 6^4\}$ topology for **Zn4**, and a one-dimensional “wave-like” chains for **Zn5**. The emission maximum wavelengths of complexes **Zn1**–**Zn5** can be tuned in a large range of 461–592 nm due to the electron donating ability and conjugated system of the ligands. After doping complex **Zn3** with PMMA matrix, PMMA-supported doped polymer film materials was obtained, which displays excellent green luminescent properties with enhanced luminescent intensities and thermal stability. Thus the as-prepared Zn(II) complexes can be used in the pursuit of application in farm plastic-film with optical transfer function.

Acknowledgements

This work was supported by National Natural Science Foundation of China (Grant 21371040 and 21571042), the National Key Basic Research Program of China (973 Program, No. 2013CB632900).

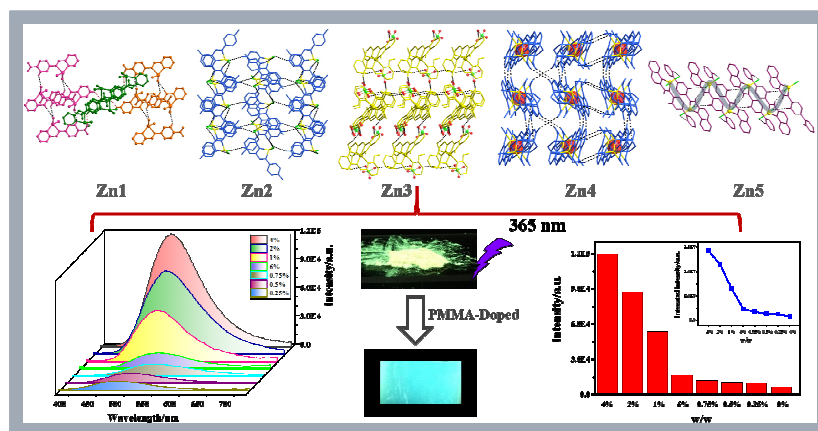
Note and references

- J. W. Steed, J. L. Atwood, *Supramolecular Chemistry*, John Wiley & Sons Ltd, Chichester, UK, 2000.
- W. Y. Wong, L. Liu and J. X. Shi, *Angew. Chem., Int. Ed.*, 2003, **42**, 4064–4068.
- W. Y. Wong, *Coordin. Chem. Rev.*, 2005, **249**, 971–997.
- J. Mei, N. L. C. Leung, R. T. K. Kwok, J. W. Y. Lam and B. Z. Tang, *Chem. Rev.*, 2015, **115**, 11718–11940.
- G. Consiglio, I. P. Oliveri, S. Failla and S. D. Bella, *Inorg. Chem.*, 2016, **55**, 10320–10328.
- J. Tang, Y. B. Cai, J. Jing and J. L. Zhang, *Chem. Sci.*, 2015, **6**, 2389–2397.
- J. G. Sun, Y. C. Liu, L. Y. Jin, T. Chen and B. Z. Yin, *Chem. Commun.*, 2016, **52**, 768–771.
- T. Han, X. G. Gu, J. W. Y. Lam, A. C. S. Leung, R. T. K. Kwok, T. Y. Han, B. Tong, J. B. Shi, Y. P. Dong and B. Z. Tang, *J. Mater. Chem. C*, 2016, **4**, 10430–10434.
- L. L. Han, T. P. Hu, K. Mei, Z. M. Guo, C. Yin, Y. X. Wang, J. Zheng, X. P. Wang and D. Sun, *Dalton Trans.*, 2015, **44**, 6052–6061.
- S. Yuan, Y. K. Deng and D. Sun, *Chem. Eur. J.*, 2014, **20**, 10093–10098.
- W. G. Lu, Z. W. Wei, Z. Y. Gu, T. F. Liu, J. Park, J. Park, J. Tian, M. W. Zhang, Q. Zhang, T. Gentle III, M. Bosch and H. C. Zhou, *Chem. Soc. Rev.*, 2014, **43**, 5561–5593.
- L. Fu, M. Pan, X. J. Kuang, C. Yan, K. Li, S. C. Wei and C. Y. Su, *J. Mater. Chem. A*, 2013, **1**, 8575–8580.
- X. L. Hu, C. Qin, X. L. Wang, K. Z. Shao and Z. M. Su, *Chem. Commun.*, 2015, **51**, 17521–17524.
- Y. Q. Jiao, H. Y. Zang, X. L. Wang, E. L. Zhou, B. Q. Song, C. G. Wang, K. Z. Shao and Z. M. Su, *Chem. Commun.*, 2015, **51**, 11313–11316.
- Q. Y. Yang, M. Pan, S. C. Wei, K. Li, B. B. Du and C. Y. Su, *Inorg. Chem.*, 2015, **54**, 5707–5716.
- A. Ali, G. Hundal, and R. Gupta, *Cryst. Growth Des.*, 2012, **12**, 1308–1319.
- D. Natale and J. C. Mareque-Rivas, *Chem. Commun.*, 2008, 425–437.
- M. Nishio, *CrystEngComm*, 2004, **6**, 130–158.
- J. S. Field, O. Q. Munro and B. P. Waldron, *Dalton Trans.*, 2012, **41**, 5486–5496.
- J. M. Lin, Y. X. Qiu, W. B. Chen, M. Yang, A. J. Zhou, W. Dong and C. E. Tian, *CrystEngComm*, 2012, **14**, 2779–2786.
- R. F. Semeniuc, T. J. Reamer and M. D. Smith, *New J. Chem.*, 2010, **34**, 439–452.
- G. Mahmoudi, V. Stiliniović, M. S. Gargari, A. Bauzá, G. Zaragoza, W. Kaminsky, V. Lynch, D. Choquesillo-Lazarte, K. Sivakumar, A. A. Khandari and A. Frontera, *CrystEngComm*, 2015, **17**, 3493–3502.
- W. K. Lo, W. K. Wong, W. Y. Wong and J. P. Guo, *Eur. J. Inorg. Chem.*, 2005, **2005**, 3950–3954.
- Y. H. Wen, T. L. Sheng, S. M. Hu, Y. L. Wang, C. H. Tan, X. Ma, Z. Z. Xue, Y. Wang and X. T. Wu, *CrystEngComm*, 2013, **15**, 2714–2721.
- M. Gaeta, I. P. Oliveri, M. E. Fragalà, S. Failla, A. D'Urso, S. D. Bella and R. Purrello, *Chem. Commun.*, 2016, **52**, 8518–8521.
- A. Gogoi, S. Mukherjee, A. Ramesh and G. Das, *Anal. Chem.*, 2015, **87**, 6974–6979.
- M. D. Yang, Y. Zhang, W. J. Zhu, H. Z. Wang, J. Huang, L. H. Cheng, H. P. Zhou, J. Y. Wu and Y. P. Tian, *J. Mater. Chem. C*, 2015, **3**, 1994–2002.
- Z. P. Zheng, Y. J. Ou, X. J. Hong, L. M. Wei, L. T. Wan, W. H. Zhou, Q. G. Zhan and Y. P. Cai, *Inorg. Chem.*, 2014, **53**, 9625–9632.
- P. Chakraborty, J. Adhikary, S. Samanta, I. Majumder, C. Massera, D. Escudero, S. Ghosh, A. Bauza, A. Frontera and D. Das, *Dalton Trans.*, 2015, **44**, 20032–20044.
- R. Jia, H. F. Li, P. Chen, T. Gao, W. B. Sun, G. M. Li and P. F. Yan, *CrystEngComm*, 2016, **18**, 917–923.
- Q. H. Meng, P. Zhou, F. Song, Y. B. Wang, G. L. Liu and H. Li, *CrystEngComm*, 2013, **15**, 2786–2790.
- Z. Zhang, W. Feng, P. Su, X. Lu, J. Song, D. Fan, W. K. Wong, R. A. Jones and C. Su, *Inorg. Chem.*, 2014, **53**, 5950–5960.
- T. Hofbeck, U. Monkowius and H. Yersin, *J. Am. Chem. Soc.*, 2015, **137**, 399–404.
- M. J. Leidl, V. A. Krylova, P. I. Djurovich, M. E. Thompson and H. Yersin, *J. Am. Chem. Soc.*, 2014, **136**, 16032–16038.
- W. Li, P. Yan, G. Hou, H. Li and G. Li, *Dalton Trans.*, 2013, **42**, 11537–11547.
- Y. W. Dong, R. Q. Fan, P. Wang, L. G. Wei, X. M. Wang, H. J. Zhang, S. Gao, Y. L. Yang and Y. L. Wang, *Dalton Trans.*, 2015, **44**, 5306–5322.
- R. Z. Lakowicz, *Principles of fluorescence spectroscopy* (2nd Ed); Klumer Academic/Plenum Publisher: New York, 1999.
- H. Liu, T. Ye and C. Mao, *Angew. Chem., Int. Ed.*, 2007, **46**, 6473–6475.
- S. Chen, Y. K. Wu, Y. Zhao and D. N. Fang, *RSC Adv.*, 2015, **5**, 72009–72018.
- Sheldrick, G. M. *SHELXTL NT Crystal Structure Analysis Package, Version 5.10, Bruker AXS*, Analytical X-ray System, Madison, WI, 1999.
- P. Baran, R. Boca, M. Breza, H. Elias, H. Fuess, V. Jorik, R. Klement and I. Svoboda, *Polyhedron*, 2002, **21**, 1561–1571.
- X. Gong, Y. Y. Ge, M. Fang, Z. G. Gu, S. R. Zheng, W. S. Li, S. J. Hu, S. B. Li and Y. P. Cai, *CrystEngComm*, 2011, **13**, 6911–6915.
- M. Shakir, M. Azam, Y. Azim, S. Parveen and A. U. Khan, *Polyhedron*, 2007, **26**, 5513–5518.
- J. Kumar, M. J. Sarma, P. Phukan and D. K. Das, *Dalton Trans.*, 2015, **44**, 4576–4581.
- A. W. Addison, T. N. Rao, J. Reedijk, J. van Rijn and G. C. Verschoor, *J. Chem. Soc., Dalton Trans.*, 1984, 1349–1356.
- L. Yang, D. R. Powell and R. P. Houser, *Dalton Trans.*, 2007, 955–964.

- 47 Y. W. Dong, R. Q. Fan, P. Wang, L. G. Wei, X. M. Wang, S. Gao, H. J. Zhang, Y. L. Yang and Y. L. Wang, *Inorg. Chem.*, 2015, **54**, 7742–7752.
- 48 M. Franks, A. Gadzhieva, L. Ghandhi, D. Murrell, A. J. Blake, E. S. Davies, W. Lewis, F. Moro, J. McMaster and M. Schröder, *Inorg. Chem.*, 2013, **52**, 660–670.
- 49 Y. W. Dong, R. Q. Fan, X. M. Wang, P. Wang, H. J. Zhang, L. G. Wei, W. Chen and Y. L. Yang, *Cryst. Growth Des.*, 2016, **16**, 3366–3378.
- 50 F. Wu, H. Tong, Z. Li, W. Lei, L. Liu, W. Y. Wong, W. K. Wong and X. Zhu, *Dalton Trans.*, 2014, **43**, 12463–12466.
- 51 F. Wu, J. Li, H. Tong, Z. Li, C. Adachi, A. Langlois, P. D. Harvey, L. Liu, W. Y. Wong, W. K. Wong and X. Zhu, *J. Mater. Chem. C*, 2015, **3**, 138–146.
- 52 R. Y. Huang, H. Jiang, C. H. Zhu and H. Xu, *RSC Adv.*, 2016, **6**, 3341–3349.
- 53 C. X. Ding, X. Rui, C. Wang and Y. S. Xie, *CrystEngComm*, 2014, **16**, 1010–1019.
- 54 X. Shi, G. S. Zhu, Q. R. Fang, G. Wu, G. Tian, R. W. Wang, D. L. Zhang, M. Xue and S. L. Qiu, *Eur. J. Inorg. Chem.*, **2004**, 185–191.
- 55 C. Y. Xu, Q. Q. Guo, X. J. Wang, H. W. Hou and Y. T. Fan, *Cryst. Growth Des.*, 2011, **11**, 1869–1879.
- 56 B. X. Dong and Q. Xu, *Cryst. Growth Des.*, 2009, **9**, 2776–2782.
- 57 Y. H. Wu, L. Chen, J. Yu, S. L. Tong and Y. Yan, *Dyes and Pigments*, 2013, **97**, 423–428.
- 58 J. N. Demas and G. A. Crosby, *J. Phys. Chem.*, 1971, **75**, 991–1024.
- 59 C. Maxim, F. Tuna, A. M. Madalan, N. Avarvari and M. Andruh, *Cryst. Growth Des.*, 2012, **12**, 1654–1665.
- 60 H. Mandal, S. Chakrabarty and D. Ray, *RSC Adv.*, 2014, **4**, 65044–65055.
- 61 K. D. Murugan and P. Natarajan, *Eur. Polym. J.*, 2011, **47**, 1664–1675.
- 62 Y. Song, R. Q. Fan, P. Wang, X. M. Wang, S. Gao, X. Du, Y. L. Yang and T. Z. Luan, *J. Mater. Chem. C*, 2015, **3**, 6249–6259.

Different Conjugated System Zn(II) Schiff Base Complexes: Supramolecular Structure, Luminescent Properties and Application in PMMA-Doped Hybrid Material

Yu-Wei Dong, Rui-Qing Fan,* Wei Chen, Hui-Jie Zhang, Yang Song, Xi Du, Ping Wang, Li-Guo Wei, and Yu-Lin Yang,*



Supramolecular structures and luminescent properties of Zn(II) Schiff base complexes based on the different conjugated system have been studied in detail. Complex **Zn3** is incorporated into PMMA representing high performance materials.